A new methodology for anisotropic yield surface description using model order reduction techniques and invariant neural network

Chady Ghnatios, Oana Cazacu, Benoit Revil-Baudard, Francisco Chinesta

A new methodology for anisotropic yield surface description using model order reduction techniques and invariant neural network

Chady Ghnatios [a,*], Oana Cazacu [b], Benoit Revil-Baudard [b], Francisco Chinesta [c]

[a] SKF research chair @ arts et métiers institute of technology PIMM Laboratory, Arts et Métiers institute of technology, CNRS, CNAM, HESAM Université, 151 Boulevard de l'Hôpital, 75013 Paris, France
[b] Department of Materials Science and Engineering, University of Arizona, 1235 James E. Rogers Way, Tucson, AZ 85719, USA
[c] PIMM Laboratory, Arts et Métiers institute of technology, CNRS, CNAM, HESAM Université, 151 Boulevard de l'Hôpital, 75013 Paris, France

ARTICLE INFO

Keywords:
Model reduction
Machine learning
Yield surface
Generic material model

ABSTRACT

In this paper, we present a general methodology that we call spectral neural network (SNN) which enables to generate automatically knowing a few datapoints (eight at most), a sound and plausible yield surface for any variations of a given anisotropic material, e.g. batches of the same material or same type of material produced by a different supplier. It relies on the use of a reliable parametrization of a performant analytic orthotropic yield function for the generation of a large database of yield surface shapes and the singular value decomposition method to create a reduced basis. For a specific material, a surrogate model for the reduced basis coordinates is further constructed using few additional datapoints. The dense neural network is built such as to ensure that the invariance requirements dictated by the material symmetry as well as the convexity of the yield surface are automatically enforced. The capabilities of this new methodology are demonstrated for hexagonal closed packed materials titanium materials, which are known to be particularly challenging to model due to their anisotropy and tension–compression asymmetry. Furthermore, we show that the SNN methodology can be extended such as to include variations of multiple materials of vastly different plastic behavior and yield surface shapes. The in-depth analysis presented reveals the benefits and limits of the hybrid data-driven models for description of anisotropic plasticity.

1. Introduction

There have been increased interest in using machine learning methods to guide in the efforts to describe the mechanical behavior of materials. For the case when the behavior can be approximated by linear or non-linear one-to-one mappings, the success of such methods has been demonstrated in Kirchdoerfer and Ortiz (2016) and Allen and Tkatchenko (2022). However, using such methods to model plastic behavior poses additional challenges associated with the need to determine if for a given stress state the response is elastic or permanent deformation occurs upon unloading. This is a very complex task, given that it requires the definition of a 6-dimensional surface in the stress space, or a 5-dimensional surface in the case of pressure-independent materials (e.g. metallic materials). Moreover, the experimental data available is generally very scarce, and most of it corresponds to uniaxial loadings (only one stress component is different from zero). More complex loadings, involving both shear and normal stress components are either difficult and expensive to instrument and perform, or cannot be accessible at all because the necessary testing devices remain to be discovered. Moreover, due to the intrinsic symmetries of the crystal lattice or processing (e.g. rolling), certain metallic materials

* Corresponding author.
E-mail address: chady.ghnatios@ensam.eu (C. Ghnatios).

display anisotropy in plastic properties. For such materials, just the quantification of the anisotropy in uniaxial tension requires a substantial increase in the number of physical tests that need to be conducted. Therefore, a purely data-driven approach to modeling the yield surface of any given material is not at hand, with the currently available technology.

On the other hand, for certain materials/microstructures there exist highly performant analytic yield functions. For isotropic materials with face-centered cubic (FCC) or body-centered cubic (BCC) lattice, the von Mises yield function (Mises, 1928) is adequate (see Hill, 1948). The extension of the von Mises yield function such as to account for orthotropic symmetries induced by fabrication processes was reported by Hill (1948, 1979). This formulation has proven to be quite satisfactory for typical aluminum and steel alloys (Cazacu et al., 2019). To better account for the experimentally observed response of newer, more advanced metallic alloys, the traditional approach has been to propose new mathematical expressions involving more anisotropy parameters. For example, the orthotropic yield function proposed by Barlat et al. (2005), called Yld2004, involves 18 anisotropy parameters whereas Hill (1948) involves 6 anisotropy parameters (Hill, 1948).

Ibáñez et al. (2019) posed and addressed the following fundamental research question: starting from a given analytic yield function, is it possible to develop a data-driven model correction which would be satisfactorily close to a more complex analytic yield function? These authors showed that a correction to the Hill model such as to satisfy Yld2004 can be built in a fully automatic fashion. A non-linear sparse identification technique was developed to construct the response surface for the error with respect to the Yld2004 yield function.

For hexagonal-closed packed (HCP) materials that are anisotropic, pressure-insensitive, but exhibit difference in response between tension and compression, none of the analytic yield functions developed for FCC and BCC materials such as Hill (1948) or Yld2004 can describe the yielding response (Hill, 1948; Barlat et al., 2005). Simply increasing the number of anisotropy parameters in these latter formulations would not do. This is because these latter yield functions are even functions of the stress tensor, so by construction the response in tension is the same as the response in compression. New mathematical expressions were developed to describe simultaneously the anisotropy and tension–compression symmetry by Cazacu and Barlat (2004) and Cazacu et al. (2006).

To obtain a data-driven correction for the Hill (1948) yield function that would account for both orthotropy and the tension–compression asymmetry in yielding of HCP materials, Fuhg et al. (2022a,b) used for training synthetic datasets obtained using the Cazacu and Barlat (2004) yield function. These datasets included both biaxial compressive and tensile yield stresses as well as uniaxial yield stresses along several directions. Several machine learning approaches were used for building the surrogate model for the discrepancy between the Hill (1948) and the Cazacu and Barlat (2004) yield surfaces. Irrespective of the machine learning approach used, the authors imposed convexity of the model correction. It was shown that with constrained gaussian process regression and neural network approaches, the hybrid model describes both the anisotropy in uniaxial yield stresses and the shape of the Cazacu and Barlat (2004) surface. However, the hybrid model cannot capture neither the range of the Lankford coefficients (i.e. the ratios between the transverse plastic strains under uniaxial tension along a given direction) or the orientation dependence of the Lankford coefficients of the given material. Also, given that Hill's yield function is convex irrespective of the parametrization, and that the "true" yield surface should be convex, the correction does not necessarily need to be convex.

It is worth noting that in the aforementioned studies, in order to capture the yield function of a particular anisotropic material, it was sought a data-driven enhancement of an anisotropic yield function (Hill's 1948). One of the objectives of this paper is to investigate whether it is possible using machine learning approaches to enhance an isotropic yield function, namely the von Mises yield function such as to describe anisotropic yielding. Because of the scarcity of experimental data, of particular interest is to establish the minimum physical tests required to ensure that the key features of the plastic behavior are automatically taken into account. In contrast to previous studies (Ibáñez et al., 2019; Fuhg et al., 2022a), in this work, a dense neural network is constructed such as to ensure that the invariance requirements dictated by the material symmetry (i.e. orthotropy) are automatically satisfied. Moreover, special attention is given to enforce that the yield surface is convex, through penalizing the change of curvature. We also ensure the fulfillment of all the knowledge available concerning the curvature of the yield surface. In addition to ensure that the key physics are embedded, enforcing these latter constraints guarantees the robustness and efficiency needed for possible inclusion and use of the hybrid model in a FE solver.

Another key objective of this work is to develop a framework that would enable to predict how small variabilities in processing may affect the overall mechanical performance. Basically, if for a type of material, e.g. a commercially pure titanium (CP-Ti), a reliable parametrization of an analytic yield function exists, the idea is to take advantage of this knowledge to generate, in an automatic fashion, the yield surface for another batch of the same material or for a material of the same composition produced by a different supplier.

With this in mind, we propose here a new methodology which takes advantage of existing performant yield functions and the benefits brought about by machine learning methods. The approach that we introduce relies on a database consisting of multiple realizations of the yield surface of a particular material using the Cazacu et al. analytic yield function (Cazacu et al., 2006), creating a reduced basis, and further developing a surrogate model using only few measurements for a specific material.

The methodology and framework developed is applied to anisotropic HCP materials, because of their technological importance and the challenges that they pose in terms of both mechanical characterization and modeling. Indeed, these materials, for example titanium materials have outstanding mechanical properties such as high strength to weight ratio, corrosion resistant, biocompatibility. Considering the extreme environments in which components made of such materials operate, it is critical to have a better understanding of how small variabilities associated with material fabrication may affect their performance.

The paper is organized as follows. In Section 2, we present the SNN methodology for constructing the reduced basis and surrogate for the data-driven correction to the von Mises yield function, and its application to the automatic generation of the yield surface for anisotropic CP-Ti materials. Next, we investigate whether it is possible to extend this methodology such as to obtain a response

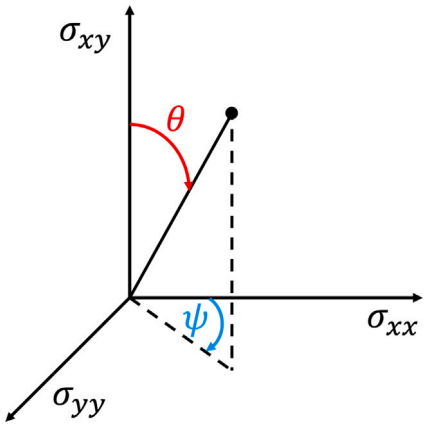

Fig. 1. The spherical coordinates used in this work.

surface that approximates the Cazacu et al. (2006) (CPB) yield surface of titanium-like materials of various levels of anisotropy (Revil-Baudard et al., 2021). To this end, we create a larger database of yield surface shapes from variations around the CPB yield surfaces of two materials: an anisotropic CP-Ti and an isotropic material (Section 3).

The ultimate challenge consists in generating the yield surface of any HCP material using only a few data points. For this purpose, we create a large database consisting of realizations around four different materials, including two HCP materials of drastically different asymmetry and anisotropy (Section 4). Specifically, training samples are generated by considering 15% variation around the parameters of an anisotropic commercially pure titanium material, an anisotropic magnesium alloy, an isotropic material displaying tension–compression asymmetry, and a von Mises material (Section 5). The main findings and key conclusions are discussed in Section 6.

2. Methodology

In this paper, we aim at modeling the shape of the yield surface of anisotropic HCP metallic materials. We will consider the case of plane stress, although the approach and methodology that we develop in this paper for describing the shape of the yield surface can be extended to 6-D loadings. Let us denote Oxyz, the coordinate system associated with the axes of orthotropy of the material. As an example, for a thin rolled metallic sheet, x, y, z axes correspond to the rolling (RD), transverse (TD), and through-thickness direction (TT), respectively, i.e. the only non-zero stresses are σ_{xx}, σ_{yy} and σ_{xy}. This stress state can be represented as (Ibáñez et al., 2019):

$$\begin{cases} \sigma_{xx} = \mathbf{r}(\theta,\psi)\cdot cos\psi\cdot sin\theta \\ \sigma_{yy} = \mathbf{r}(\theta,\psi)\cdot sin\psi\cdot sin\theta \\ \sigma_{xy} = \mathbf{r}(\theta,\psi)\cdot cos\theta \end{cases} \tag{1}$$

where $\psi \in [0;2\pi]$ and $\theta \in [0;\pi]$, with $\mathbf{r}(\psi,\theta)$ fully defining the shape of the yield surface. The convention used in spherical coordinates is illustrated in Fig. 1.

The physical constraints to be enforced in order to generate a sound yield surface are:

- convexity,
- the symmetry requirements associated to orthotropy.

Specifically, the orthotropy of the material dictates that the yield surface should be symmetric with respect to the plane for which $\sigma_{xy} = 0$.

As previously mentioned, for orthotropic HCP materials modeling the shape of their yield surface is very challenging. In this work, we propose to use model order reduction techniques to address efficiently the construction of a reduced basis for the yield surface, starting from the analytical yield surfaces of specified materials. For the sake of completeness, the CPB yield function is briefly presented in the following.

2.1. Cazacu et al. (2006) yield function

To construct large databases for HCP materials, we use the quadratic CPB orthotropic yield function (Cazacu et al., 2006):

$$F(\boldsymbol{\sigma}) = \left(|\Sigma_1| - k\cdot\Sigma_1\right)^a + \left(|\Sigma_2| - k\cdot\Sigma_2\right)^a + \left(|\Sigma_3| - k\cdot\Sigma_3\right)^a, \tag{2}$$

with k being a material parameter and Σ_1, Σ_2, Σ_3 denoting the eigenvalues of the transformed stress tensor:

$$\Sigma = \mathbf{C} \cdot \mathbf{s} \tag{3}$$

In Eq. (3), $\mathbf{C}$ is a fourth-order symmetric and orthotropic tensor that describes the material's anisotropy, and $\mathbf{s}$ denotes the stress deviator. Therefore, in the Cartesian coordinate system associated with the orthotropy axes, the tensor $\mathbf{C}$ is represented by the following 6×6 matrix (Voigt notations) :

$$\mathbf{C} = \begin{bmatrix} C_{11} & C_{12} & C_{13} & 0 & 0 & 0 \\ C_{21} & C_{22} & C_{23} & 0 & 0 & 0 \\ C_{31} & C_{32} & C_{33} & 0 & 0 & 0 \\ 0 & 0 & 0 & C_{44} & 0 & 0 \\ 0 & 0 & 0 & 0 & C_{55} & 0 \\ 0 & 0 & 0 & 0 & 0 & C_{66} \end{bmatrix} \tag{4}$$

Due to the homogeneity in stresses of the yield function, the anisotropy coefficients can be scaled by C_{11}, or equivalently, one can set $C_{11} = 1$. Therefore, for general loadings this orthotropic yield criterion involves eight independent anisotropy coefficients, and the parameter k. Note that if $k \neq 0$, the yield function is not an even function, and consequently the predicted yielding in tension is different than that in compression (tension–compression asymmetry).

Remark. For a material that is isotropic, $\mathbf{C} = \mathbf{I}_4$, where $\mathbf{I}_4$ denotes the 4th order symmetric identity tensor. Moreover, for an isotropic material with the same response in tension and compression, the parameter $k = 0$ and the CPB yield function reduces to the classic von Mises yield criterion:

$$s_1^2 + s_2^2 + s_3^2 = (2/3)\sigma_T^2, \tag{5}$$

where s_1, s_2 and s_3 are the principal values of the stress deviator $\mathbf{s}$, and σ_T is the tensile yield stress in any orientation.

2.2. Hybrid modeling of the yield surface of an anisotropic HCP material, starting from the isotropic von mises yield surface

When the difference between the considered yield model and a given state of the art yield surface remains quite small, the modeling of the gap, within an hybrid setting, remains an appealing approach.

2.2.1. Modeling approach

We assume that the true yield surface is described by the CPB yield function given by Eq. (2) and that the starting isotropic yield function is the classical von Mises. We seek to build a response surface for the model correction, i.e:

$$\mathbf{r}_{error}(\theta, \psi) = \mathbf{r}_{CPB}(\theta, \psi) - \mathbf{r}_{VM}(\theta, \psi) \tag{6}$$

where $\mathbf{r}_{CPB}(\theta, \psi)$ and $\mathbf{r}_{VM}(\theta, \psi)$ define in the 3D stress space, the CPB and the von Mises yield surface, respectively (see Eqs. (1), (2) and (6)). Moreover, the sought model correction should be applicable to a large range of materials, namely small variations of a selected material or the same type of material as the selected one.

To this end, we propose as a first step to generate a large database by random sampling the CPB anisotropy parameters of a given material while satisfying the orthotropy of the fourth-order tensor, $\mathbf{C}$, and preserving as a constraint $C_{11} = 1$ (see Eq. (4)). Specifically, N random samplings are generated using a small variation around given values (e.g. $\pm 15\%$ variation) and this set is divided into two parts. The first n_1 samples with $n_1 < N$ are used to build the reduced basis and the surrogate model. The remaining $n_2 = N - n_1$ computed CPB surfaces that were not used for the construction of the reduced basis or for training of the surrogate model, but will serve to validate the approach after the convergence of the training.

2.2.2. Defining the reduced basis

A reduced basis is used in model reduction technique to create a global approximation basis which acts on the complete domain (Chinesta et al., 2011). In this work, the reduced basis is found using the singular value decomposition (SVD) method:

$$[\mathbf{U}, \mathbf{\Lambda}, \mathbf{W}] = svd(\mathbf{r}_{error}^{n_1}) \tag{7}$$

The matrices $\mathbf{U}$ and $\mathbf{W}$ consists of the space and discrepancy mode shapes, respectively while $\mathbf{\Lambda}$ is a diagonal matrix containing the singular values of the decomposition. The reduced basis $\mathbf{V}$ is obtained by retaining only the n highest singular values in the diagonal matrix and their corresponding vectors in $\mathbf{U}$. Noting that $\mathbf{V}$, the resulting reduced basis, consists of the first n vectors of $\mathbf{U}$, one can now write:

$$\mathbf{r}_{error}(\theta, \psi) \approx \sum_{i=1}^{n} V_i \cdot \zeta_i, \tag{8}$$

with ζ_i being the n reduced coordinates defining the error surface. A surrogate model is built to predict the reduced coordinates from the available test measurements, i.e $\boldsymbol{\zeta} = h(\mathbf{X})$, where $\mathbf{X}$ is the vector of available experimental measurements. Therefore, once the reduced basis $\mathbf{V}$ is available, the yield surface of a given material $\mathbf{r}_{error}(\theta, \psi)$, can be generated in an automatic fashion, i.e.:

$$\mathbf{r}(\theta, \psi) \approx \mathbf{r}_{VM} + \sum_{i=1}^{n} V_i \cdot \zeta_i, \tag{9}$$

2.2.3. Surrogate modeling

Special care is devoted toward enforcing the orthotropy requirements of the yield surface. Specifically, we define the surrogate model only for $\theta \in [0; \pi/2]$, the full surface being obtained by symmetry. In this manner, we ensure that yielding does not depend on the sign of the shear stress. A suitable non-linear approach to build the surrogate model h is a deep dense neural network. We choose to not consider an input-convex neural network for the following reasons:

- neither the yield surface nor its reduced coordinates $\boldsymbol{\zeta}$ are convex with respect to the experimental measurements, $\mathbf{X}$,
- the model correction to a pre-defined convex yield surface is not necessarily convex.

The network is trained using the following loss function :

$$\begin{aligned}\mathcal{L} = \sum_{k=1}^{p} \left(r_{error} - \sum_{i=1}^{n} \zeta_i V_i(\theta_k, \psi_k) \right)^2 + \lambda_1 \cdot relu\left(\frac{\partial^2 r}{\partial \theta^2} + \frac{1}{r} \frac{\partial r}{\partial \theta} \right) \\ + \lambda_2 \cdot relu\left(\frac{\partial^2 r}{\partial \psi^2} + \frac{1}{r^2 sin^2 \theta} \frac{\partial r}{\partial \psi} \right) + \lambda_3 \sum_{i=1}^{n} |\zeta_i|\end{aligned} \tag{10}$$

Note that the first sum in $\mathcal{L}$, is over the available sampling points in the (θ, ψ) domain. For example, if meshing of the domain is performed at a step of one degree in either θ or ψ, the number of available points would be $p = 90 \times 360$ points. The coefficients λ_1, λ_2 and λ_3 are regularization parameters, which multiply respectively:

- the curvature of the yield surface along θ
- the curvature of the yield surface along ψ
- the problem's parameters ζ_i

The first and second regularization terms are introduced such as to reduce the curvature variation in the domain and thus restrain the solution to a single convex variation as much as possible. It is also worth noting that the curvature is computed over the total yield surface, having a radius $\mathbf{r} = \mathbf{r}_{VM} + \sum_{i=1}^{n} \zeta_i V_i$, and not over the discrepancy surface $\mathbf{r}_{error}$, as the convexity is a property of the yield surface itself. This is because the final corrected yield surface is required to be convex, not its correction. The imposition of such a condition would lead to a convex yield surface through penalty.

The third regularization term is required because the available testing data $\mathbf{X}$ is very limited, and consequently there are more unknowns than measurements. The use of the third regularization term reduces the amplitude of the problem's coefficients and promotes sparsity and convexity of the loss function $\mathcal{L}$.

For all the examples provided in this paper, the training is performed using an in-house code, based on ADAM gradient descent algorithm (Kingma and Ba, 2014), with an adaptive learning rate.

2.3. Possible inclusion in a finite element solver

The error of the derivative of a trained surrogate model is expected to be larger than the error on that model itself, since the derivative is not included in the optimization problem when computing the model's weights. Therefore, seldom the derivative of a surrogate is used, and, if this is done, there is no guarantee of accurate representation of the derivatives.

On the other hand, for finite element calculations of plastic strains, the normal to the yield surface needs to be computed, which requires to access the derivatives with respect to the coordinates defining it. In fact, the unit normal $\mathbf{n}$ to the yield surface at any point (θ, ϕ) is defined in spherical coordinates using:

$$\mathbf{n} = \frac{1}{\sqrt{\left(\frac{\partial r}{\partial \theta}\right)^2 + \left(\frac{\partial r}{\partial \phi} \sin\theta\right)^2 + r^2}} \left(\frac{\partial r}{\partial \theta} \mathbf{e}_r + \frac{\partial r}{\partial \phi} \sin\theta \mathbf{e}_\phi \right) \tag{11}$$

It is worth noting that, in the approach developed here, the radius of the yield surface is defined as a sum of vectors (see Eq. (9)). Because the neural network training parameters do not depend on the spatial coordinates $(r, \theta; \phi)$, the derivation of the surrogate model involves only the derivatives of the mode shapes.

Indeed, the outputs of the neural network $\boldsymbol{\zeta}$ depend only on the available experimental measurements $\mathbf{X}$, and consequently the accuracy is conserved. For instance,

$$\frac{\partial \mathbf{r}}{\partial \theta} = \frac{\partial \mathbf{r}_{VM}}{\partial \theta} + \sum_{i=1}^{n} \frac{\partial V_i}{\partial \theta} \cdot \zeta_i, \tag{12}$$

This aforementioned feature makes the proposed approach more attractive than the other data-driven techniques, proposed in the literature, for describing the plastic yield surface of materials. In our approach, the derivative of the surrogate yield surface involves only derivatives of the mode shapes (see Eq. (11) and (12)). This means that the error in calculating the derivative is of the same order as the error of the surrogate yield surface. This is a clear advantage of the proposed approach over the state-of-the-art.

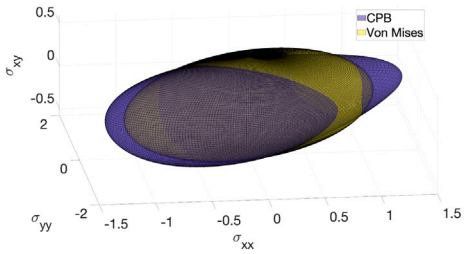

(a) Comparison of yield surfaces.

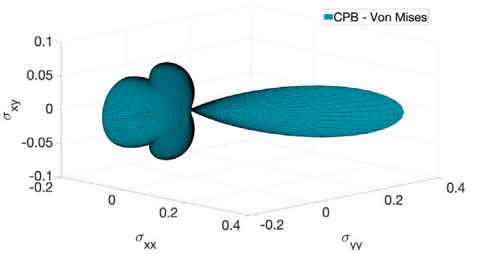

(b) The discrepancy between the two surfaces.

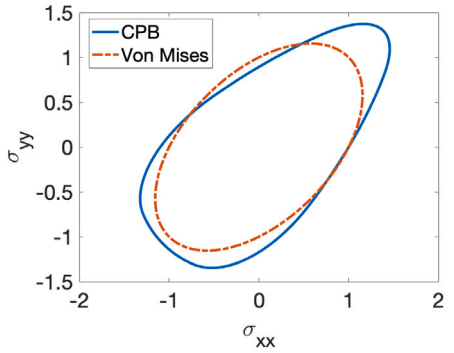

(c) Comparison of yield surfaces at $\theta = 90°$.

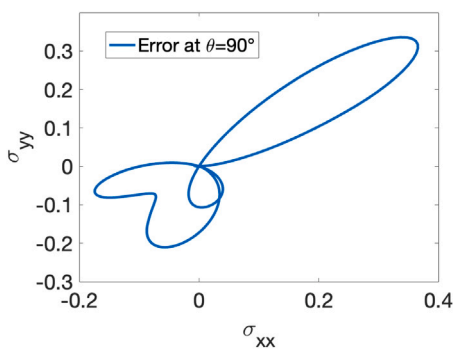

(d) The discrepancy between the two surfaces at $\theta = 90°$.

Fig. 2. Comparison between a sample CPB yield surface corresponding to anisotropy parameters within 15% of the values for a titanium T40 and the Von Mises surface. Stresses are normalized by the uniaxial tensile yield stress in the rolling direction.

3. Application to orthotropic T40 titanium

In this section, we apply the proposed approach to the description of the yield surface of CP-Ti materials. To generate the database, the CPB parameters for a sheet of commercially pure titanium, T40 reported in Revil-Baudard et al. (2021) (see Table 2 in Revil-Baudard et al., 2021), are sampled using a ±15% variation around the given values, while satisfying the symmetry of the **C** tensor and preserving as a constraint $C_{11} = 1$. Note that this material exhibits pronounced anisotropy and tension–compression asymmetry. A total of $N = 500$ CPB yield surfaces are generated by randomly sampling in the domain, among which $n_1 = 400$ samples used for the training.

As an example, in Fig. 2(a) is shown a sample CPB yield surface in the 3-D stress space along with the Von Mises yield surface while in Fig. 2(b) is depicted the discrepancy between the two surfaces (see Eq. (6)). In this and in all the plots of yield surfaces presented hereafter, the stresses are normalized by the uniaxial yield stress in tension along the RD-direction.

Fig. 2(b) clearly shows that for this realization, the discrepancy surface is not convex and could not be captured by any convex function.

Of the computed CPB yield surfaces, $n_1 = 400$ surfaces are used to generate error maps (see Eq. (6)) and the remaining 100 surfaces (labeled 401 to 500) serve for validation. The reduced basis **V** is found as described in Section 2.2.2, the rank of V being $n = 28$, which was selected based on the ratio:

$$\frac{\Lambda_n}{\Lambda_1} < \epsilon, \tag{13}$$

with $\epsilon = 10^{-6}$, and the eigenvalues Λ_i sorted using decreasing values.

One of the objectives of this paper is to investigate whether a few data points may be sufficient to capture the yield surface of a material slightly different than a given material (i.e. with small variations in plastic properties). For this purpose, using the same reduced basis V, we construct a surrogate model for the reduced coordinates using as input a very limited dataset, labeled $\mathbf{X}_5$, and a slightly larger dataset, $\mathbf{X}_8$, respectively. Specifically,

- the dataset $\mathbf{X}_5$ consists of five data points: the yield stresses in uniaxial tension and compression along the x axis (RD) and the y axis (TD), respectively, and the yield stress in equibiaxial tension;

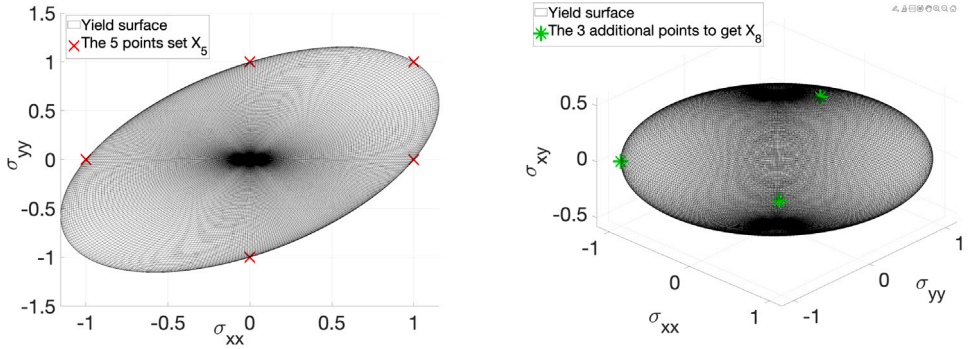

(a) Representation of the datapoints in set $\mathbf{X}_5$ on the Von Mises yield surface cross-section ($\sigma_{xy} = 0$)

(b) Representation on the 3-D Von Mises yield surface of the three additional datapoints in set $\mathbf{X}_8$

Fig. 3. Position of the selected set of datapoints $\mathbf{X}_5$ and $\mathbf{X}_8$.

Table 1
The neural network used as the surrogate model h.

Layer	Building block	Activation
1	Input layer having the size of $\mathbf{X}$	No activation
2	Dense layer with 500 neurons	*tanh*
3	Output layer having the size of $\boldsymbol{\zeta}$	*linear*

- $\mathbf{X}_8$ is a vector of eight data points, namely the previous $\mathbf{X}_5$, along with the yield stress in shear in the xy-plane, the yield stress in equibiaxial compression, and the yield stress in uniaxial tension in a direction at 45° with respect to x-axis, in the (x, y) plane.

Note that the dataset $\mathbf{X}_5$ includes only information on yielding along the symmetry directions of the material. This is the minimum amount of data necessary to characterize the anisotropy and strength differential of the HCP material. As an example, in Fig. 3 are shown these datapoints on a von Mises yield surface. To build the respective surrogate models, a dense neural network is considered, using the architecture given in Table 1.

Fig. 4 shows the predicted results using as inputs to the neural network only the five data points of $\mathbf{X}_5$ while Fig. 5 shows the predicted results obtained using $\mathbf{X}_8$. Irrespective of the dataset considered for training, the yield surface shape is correctly reproduced with an average relative error of $\mathcal{E} = 2.41\%$ when using $\mathbf{X}_5$ and $\mathcal{E} = 1.93\%$ when using $\mathbf{X}_8$, despite being very different from the von Mises one. The relative error is computed using:

$$\mathcal{E} = \frac{1}{\kappa}\sum_{i=1}^{\kappa}\left(\frac{|R_i - \hat{R}_i|}{|R_i|}\right), \tag{14}$$

with R being the correct radius and $\hat{R}$ the predicted one, κ is the total number of points on the yield surface. Although only the strength differential in the orthotropy directions and the ratio between the yield stresses in two orientations were included in training of the surrogate model, the overall anisotropy and the tension–compression asymmetry of the surface are well captured. Only the yield stresses in the vicinity of the equibiaxial stress states are slightly underpredicted. As expected, with 8 training points the precision of the algorithm increases, leading to a very accurate prediction of the curvature of the yield surface, which is essential for accurate predictions of the plastic strains. It is also to be noted that by inclusion in the training datasets yield points corresponding to loadings involving shear stresses, there is a clear improvement in the predictions of the cross-sections for $\theta = 30°$ and respectively $\theta = 60°$ (compare the results in Figs. 4(d) with 5(d)).

Next, the reduced basis is used beyond the training data set, i.e. for the description of the yield surface of a sample material among the 100 realizations kept for testing the robustness of the technique. The results obtained using the same reduced basis $\mathbf{V}$ and only 5 experimental measurements are presented in Fig. 6 while the results based on 8 experimental measurements are shown in Fig. 7, respectively. Note that irrespective of the dataset used for training the surrogate, the shape of the yield surface is captured very well, thus showing the high accuracy and the robustness of the proposed methodology. Moreover, the yield surfaces are generated within a fraction of a second on a standard laptop. Again, we can clearly see that including the three additional data points to the training dataset improves the accuracy of the surrogate model.

4. Extension of the methodology to dualmaterial database containing variations of an isotropic and orthotropic titanium

With the aim of describing the yield surface shape of both strongly textured and isotropic HCP materials, we investigate whether it is possible to extend the proposed methodology by creating a reduced basis $\mathbf{W}$ using a larger database, obtained by random sampling

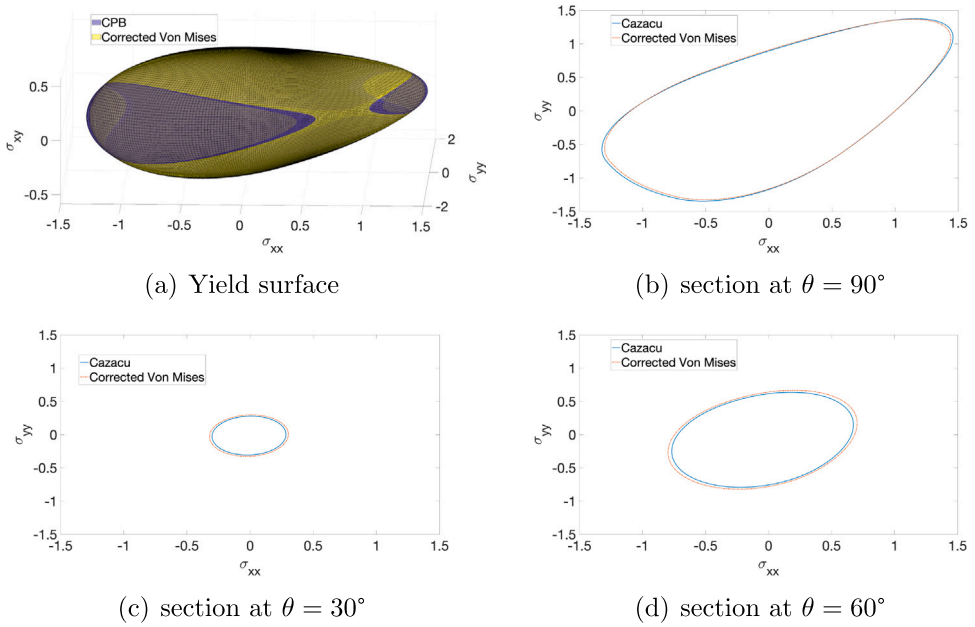

(a) Yield surface (b) section at $\theta = 90°$

(c) section at $\theta = 30°$ (d) section at $\theta = 60°$

Fig. 4. Comparison between the true (CPB) yield surface and the correction to the von Mises surface obtained with the proposed spectral neural network approach using five experimental data points, $\mathbf{X}_5$, for a selected CP-Ti material in the training database in: (a) the three-dimensional stress space, as well as several cross-sections at (b) $\theta = 90°$ ($s_{xy} = 0$); (c) $\theta = 30°$; (d) $\theta = 60°$. Stresses are normalized by the yield stress in uniaxial tension.

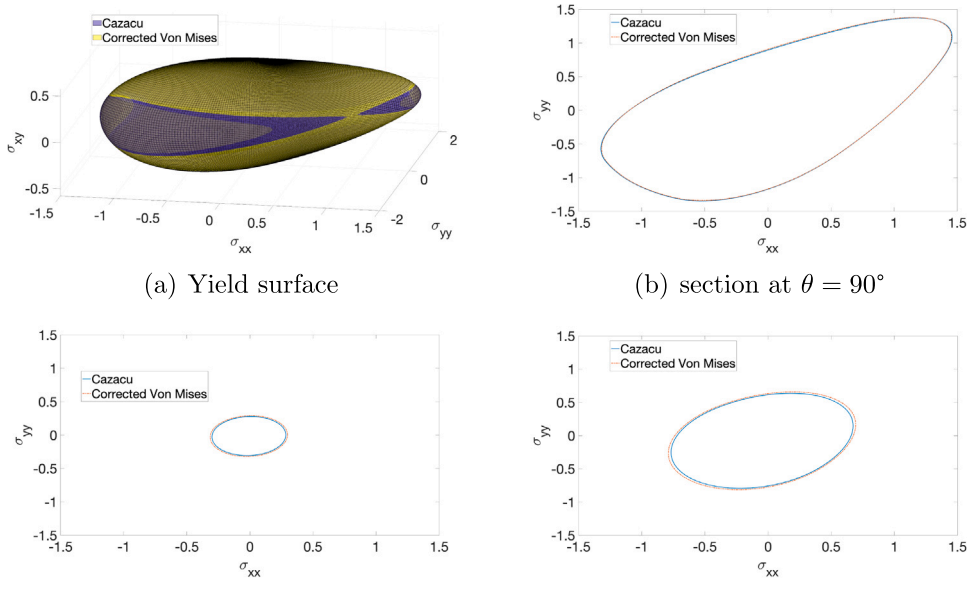

(a) Yield surface (b) section at $\theta = 90°$

(c) section at $\theta = 30°$ (d) section at $\theta = 60°$

Fig. 5. Comparison between the true (CPB) yield surface and the correction to the von Mises surface obtained with the proposed spectral neural network approach using eight experimental data points, $\mathbf{X}_8$, for a selected CP-Ti material in the training database in: (a) the three-dimensional stress space, as well as several cross-sections at (b) $\theta = 90°$ ($s_{xy} = 0$); (c) $\theta = 30°$; (d) $\theta = 60°$. Stresses are normalized by the yield stress in uniaxial tension.

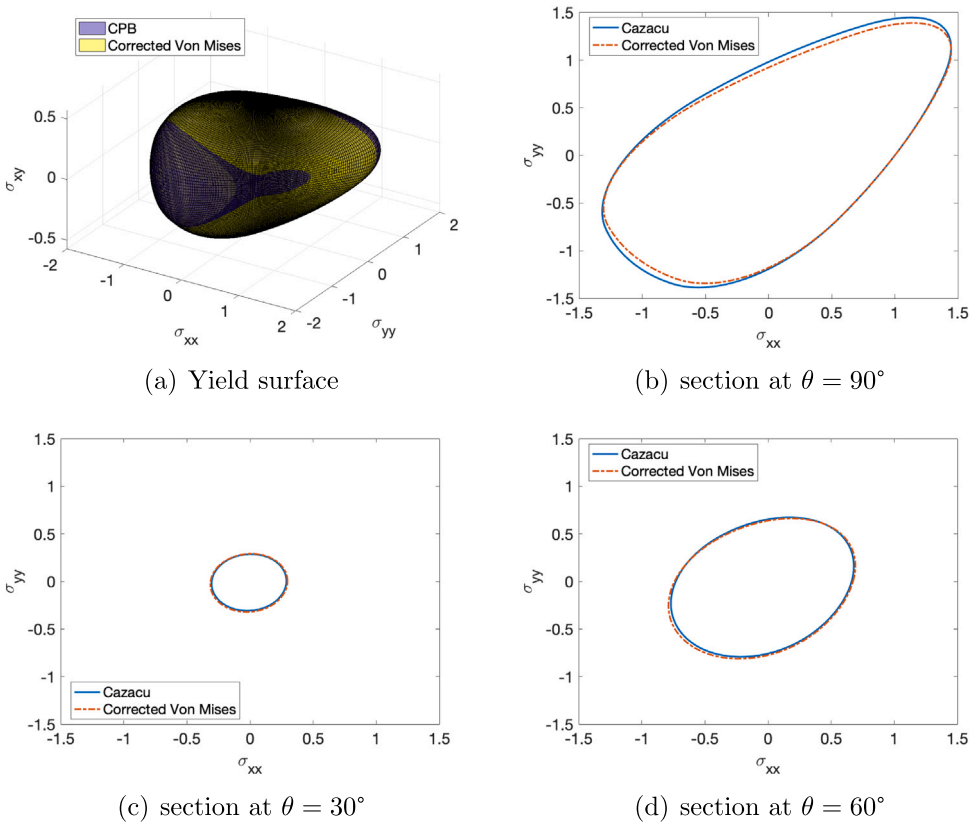

(a) Yield surface (b) section at $\theta = 90°$

(c) section at $\theta = 30°$ (d) section at $\theta = 60°$

Fig. 6. Comparison between the true (CPB) yield surface and the correction to the von Mises surface obtained from the testing set, with the proposed spectral neural network approach, using five experimental data points, $\mathbf{X}_5$, for a selected CP-Ti material in the training database in: (a) the three-dimensional stress space, as well as several cross-sections at (b) $\theta = 90°$ ($s_{xy} = 0$); (c) $\theta = 30°$; (d) $\theta = 60°$. Stresses are normalized by the yield stress in uniaxial tension.

the CPB parameters of two different materials: an almost isotropic material with tension–compression asymmetry (i.e. with $\mathbf{C} = \mathbf{I}_4$ and with k different from zero) and an orthotropic material with tension–compression asymmetry, e.g. titanium T40.

A total of 1000 CPB isotropic and anisotropic yield surfaces are constructed, namely a set of 500 snapshots are built with a variation of 15% of the parametrizations for each material. The reduced basis $\mathbf{W}$ is built using 900 surfaces, the remaining 100 surfaces are kept out of any training to validate the approach.

Let us recall that previously, we used multiple realizations of the yield surface of a single material to define the reduced basis for the correction from a predefined von Mises isotropic yield surface. In the case of a larger database which includes orthotropic and isotropic yield surfaces, the construction of the error surface with respect to the Von Mises yield surface is more complicated than fitting the CPB yield surface itself. The reduced basis $\mathbf{W}$ is determined using the singular value decomposition method, so we obtain the yield surface as:

$$\mathbf{r}(\theta, \psi) \approx \sum_{i=1}^{n} W_i \cdot \zeta_i. \tag{15}$$

Remark. It is interesting to note that in this case, the reduce basis dimension $n = 20$, which is lower than in the previous case where $n = 28$ (see Section 3). A larger number of mode shapes was required because the samplings for the T40 material have very different shapes than the von Mises yield surface (e.g. see Fig. 2).

Once the reduced basis $\mathbf{W}$ is created, surrogate modeling is done to obtain the reduced coordinates ζ_i from the available measurements. The loss function $\mathcal{L}_2$ used to train the neural network is defined as:

$$\begin{aligned}\mathcal{L}_2 = \sum_{k=1}^{p} \left(r - \sum_{i=1}^{n} \zeta_i W_i(\theta_k, \psi_k) \right)^2 + \lambda_1 \cdot relu \left(\frac{\partial^2 r}{\partial \theta^2} + \frac{1}{r} \frac{\partial r}{\partial \theta} \right) \\ + \lambda_2 relu \cdot \left(\frac{\partial^2 r}{\partial \psi^2} + \frac{1}{r^2 sin^2 \theta} \frac{\partial r}{\partial \psi} \right) + \lambda_3 \sum_{i=1}^{n} \zeta_i^2\end{aligned} \tag{16}$$

The regularization terms were adopted for the reasons explained previously see discussion following Eq. (10). It is worth mentioning that the training requires only few hours on a standard laptop. As an example, in Fig. 8 is presented the resulting

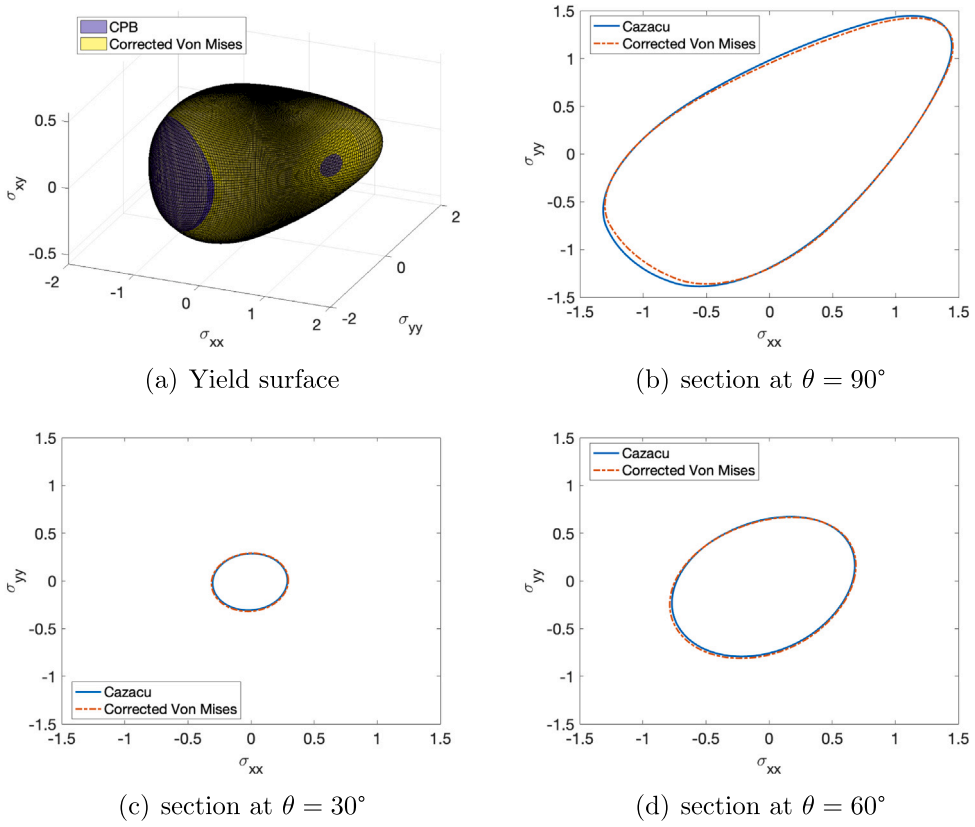

Fig. 7. Comparison between the true (CPB) yield surface and the correction to the von Mises surface obtained from the testing set, with the proposed spectral neural network approach, using eight experimental data points, $\mathbf{X}_8$, for a selected CP-Ti material in the training database in: (a) the three-dimensional stress space, as well as several cross-sections at (b) $\theta = 90°$ ($s_{xy} = 0$); (c) $\theta = 30°$; (d) $\theta = 60°$. Stresses are normalized by the yield stress in uniaxial tension.

yield surface for a material selected from the database (i.e. the testing set) obtained using only five datapoints in the training. Notice that the convexity is fully satisfied.

Fig. 9 shows the results for the same material when using $\mathbf{X}_8$ as input. The results show that the convexity is very well satisfied, and the identified yield surface is plausible as it satisfies the physical constraints. Moreover, the yield surface is computed within a fraction of a second on a standard laptop.

5. Surrogate model when disposing of a multimaterials database including realizations around four different materials

In this section, we increase the challenge, by including in the database materials with very different plastic properties. Specifically, we consider random samplings around the given parameters values for both isotropic and anisotropic materials with tension–compression asymmetry, and a von Mises material, namely:

- HCP Titanium T40
- von Mises material
- Isotropic material with different behavior in tension and compression
- HCP Magnesium

Moreover, the selected anisotropic HCP materials have a different characteristic c/a lattice, resulting in a completely different type of yield surface. Indeed, considering the HCP magnesium constitutes a very big challenge as it is known for its unconventional yield surface (Cazacu et al., 2019). The CPB parameters for the selected materials are reported in Appendix. A database consisting of 2000 realizations are created, 500 realizations for each material, with a random variation of 15% of their CPB parameters; 1900 surfaces are used for building the reduced basis and training the neural network, while the remaining 100 snapshots are kept out of any training for testing purposes. The reduced basis is built using two different methods:

- Method 1: A single reduced basis is constructed using the 1900 realizations, resulting in a basis containing 26 vectors (i.e. $n = 26$).

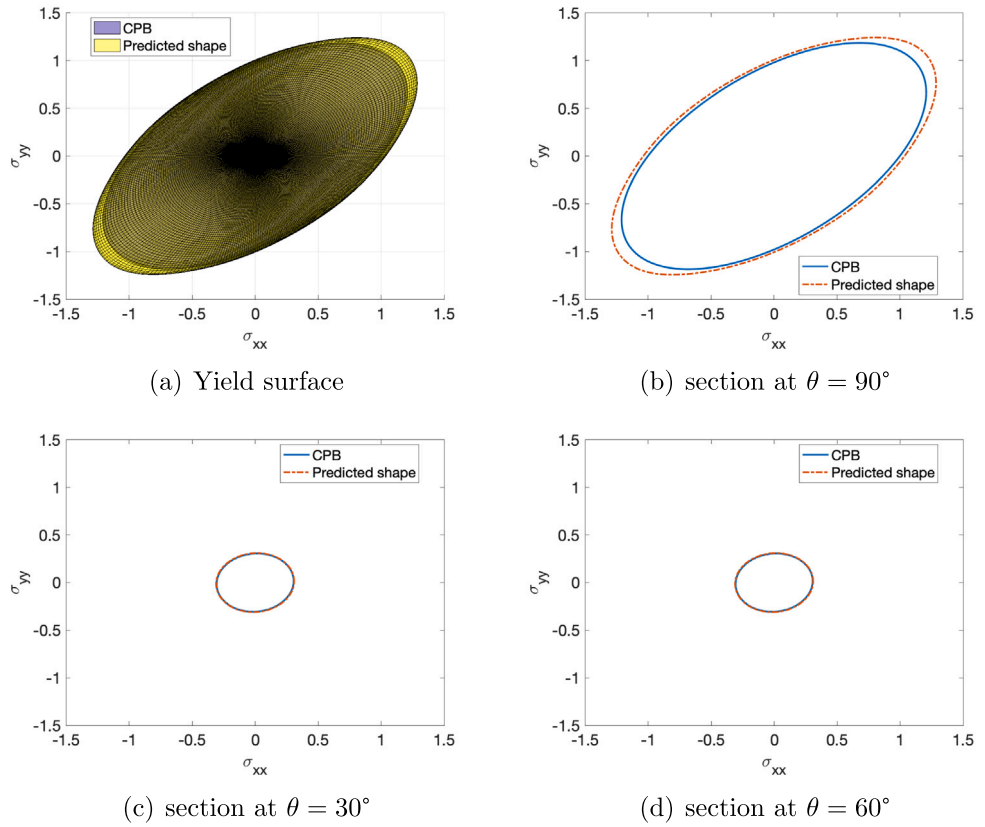

Fig. 8. Comparison between the true (CPB) yield surface and the generated yield surface for a material selected from the testing set, obtained using the proposed methodology with a database containing realizations of an isotropic and anisotropic HCP materials and five measurement points $\mathbf{X}_5$.

Table 2
Architecture of the neural network for the case of a database including realizations of four materials.

Layer	Building block	Activation
1	Input layer having the size of $\mathbf{X}$	No activation
2	Dense layer with $1500 \times n$ neurons	*tanh*
3	Output layer with n neurons	*linear*

- Method 2: A reduced basis is constructed for each material independently, then the selected vectors are concatenated. The final reduced basis dimension is $n = 44$.

Different network architectures were tested and the size of the trained neural network was increased to correctly predict the coefficients of the reduced basis. The final adopted network architecture is reported in Table 2.

The results obtained for materials from the testing set are reported in Figs. 10 and 11 for the case when training was based on 5 experimental points or 8 experimental points, respectively. Note that with both methods for constructing the reduced basis, the surrogate models trained on few data points achieved good results for the Titanium T40, the von Mises material and the isotropic material with tension–compression asymmetry, respectively. However, the surrogate model failed dramatically for the magnesium material (see Fig. 12). Note that using either method for creating the reduced basis, it is impossible to generate the correct shape of the yield surface of the magnesium material. Increasing the number of datapoints used in the training from 5 datapoints to 8 datapoints does not lead to any improvement. Note that the magnesium yield surface has a very unusual shape compared to the other 3 materials, and therefore it is possibly underrepresented in both the data-base for the training of the neural network that outputs the weights $\boldsymbol{\zeta}$, as well as in the construction of the reduced basis. It is also worth noting that the construction of the reduced basis using the second approach (method 2) did not improve the results substantially as the reduced basis size n increased dramatically, and regularization by the Lasso method was not enough to correctly suppress the useless vectors of the basis. We also note that increasing the number of available experimental data points beyond 8 did improve slightly the results for the magnesium yield surface, without leading to a satisfactory yield surface shape.

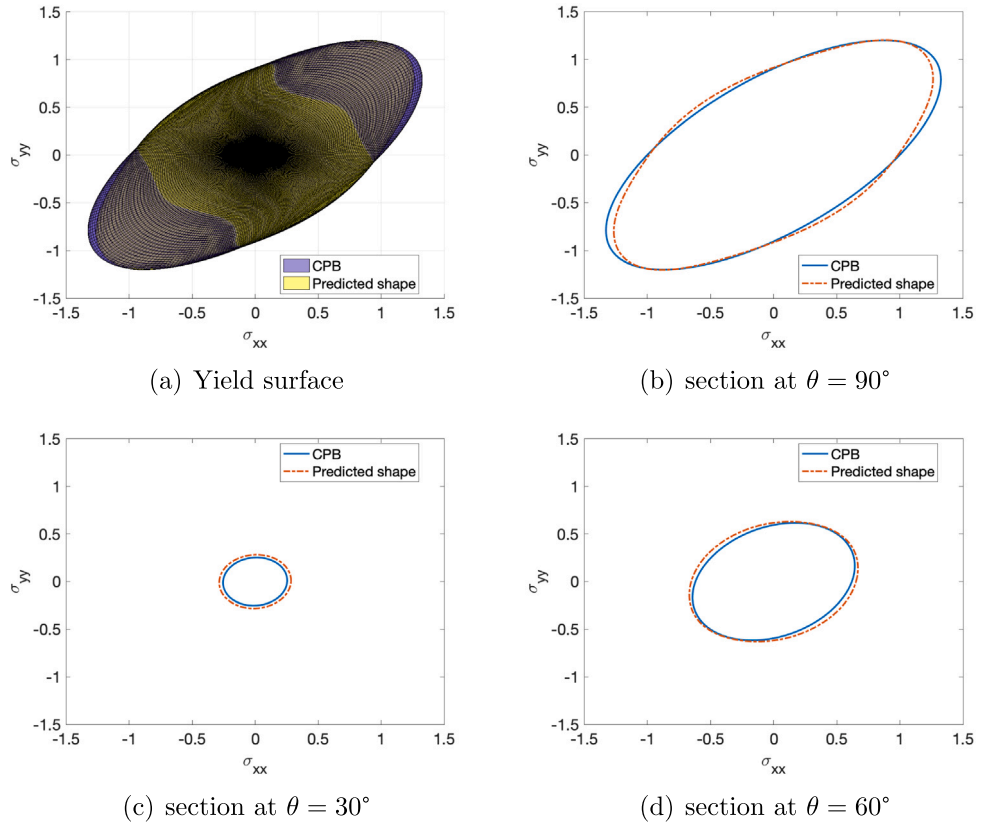

(a) Yield surface (b) section at $\theta = 90°$

(c) section at $\theta = 30°$ (d) section at $\theta = 60°$

Fig. 9. Comparison between the true (CPB) yield surface and the generated yield surface for a material selected from the testing set, obtained using the proposed methodology with a database containing realizations of an isotropic and anisotropic HCP materials and eight measurement points $\mathbf{X}_8$.

To address efficiently the magnesium case, a dedicated reduced basis and a dedicated training using only the constructed 500 realizations of the selected magnesium yield surface is considered; 400 samples yield surfaces are used for the construction of the reduced basis and training, while 100 surfaces are kept for testing. The results are shown in Fig. 13 for the case when only 5 experimental points were used for training. The generated yield surface shows an excellent similarity to the exact CPB solution.

6. Conclusions

In this work, we presented a new generic spectral neural network methodology to automatically generate a plausible yield surface for materials that are particularly challenging because of their anisotropy and tension–compression asymmetry. It takes advantage of existing performant yield functions and the benefits brought about by machine learning methods. Specifically, it relies on a reliable parametrization of a Cazacu et al. (2006) yield function for the generation of a large database of yield surface shapes from which a reduced basis can be determined using the singular value decomposition method. A dense neural network is further trained such as to determine the reduced coordinates from pre-defined datasets. To ensure that the key features of the plastic behavior are automatically taken into account, the dense neural network was built such as to ensure that the invariance requirements dictated by the material symmetries as well as the convexity of the yield surface are automatically satisfied. Moreover, this new SNN methodology has the robustness and efficiency needed for possible integration within a FE solver.

First, we illustrated the capabilities of the developed SNN methodology for constructing the data-driven correction of the von Mises yield surface such as to approximate the yield surface of an anisotropic material with tension–compression asymmetry, a CP-Ti material. Noting that the difference between two convex functions is not necessarily convex, we enforced the convexity of the yield surface itself. Moreover, the loss function used in training contains regularization terms involving the curvatures of the yield surface along the spatial coordinates.

Moreover, it was demonstrated that the SNN methodology can be used to generate in an automatic fashion the yield surface for another batch of the same material or for a material of the same composition produced by a different supplier, without having to conduct extensive testing. Furthermore, it was shown that the SNN methodology can be extended such as to obtain automatically a response surface that approximates the CPB yield surface of titanium-like materials of various levels of anisotropy. Good accuracy was achieved despite the fact that the database used for training included two materials of vastly different levels of anisotropy, namely an isotropic and an anisotropic CP-Ti, T40-titanium.

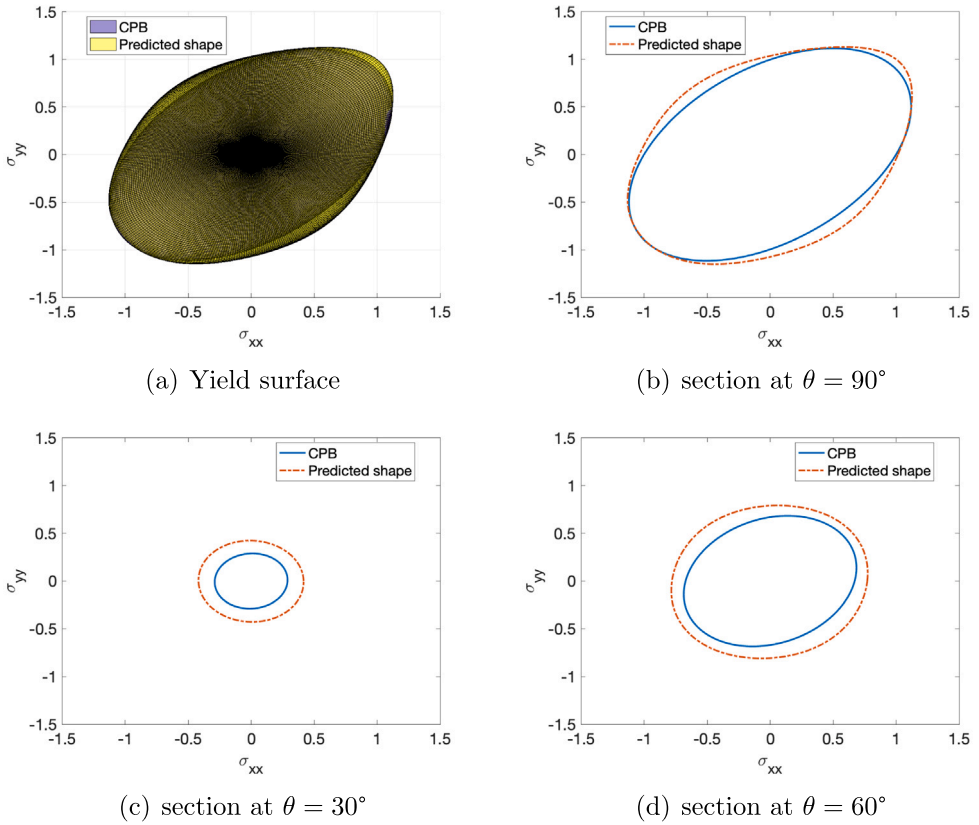

Fig. 10. Comparison between the true (CPB) yield surface and the generated yield surface for a material selected from the testing set (variant of a von Mises material), obtained using the proposed methodology with a database containing realizations of 4 HCP materials and five measurement points $\mathbf{X}_5$.

The benefits and limits of AI approaches have been investigated by further including in the database materials of vastly different plastic properties and consequently yield surface shapes, namely orthotropic titanium materials, orthotropic magnesium materials, isotropic materials with tension–compression asymmetry, and von Mises material. Two different approaches were used to determine the reduced basis. In the first approach all the variants contained in the database were used to determine the reduced basis, while in the second approach, the reduced basis was obtained by concatenating four reduced bases determined considering independently the materials present. It was shown that irrespective of the approach used to determine the reduced basis, the surrogate model achieved good results for variants of the titanium alloy and the von Mises material, but failed dramatically in the case of variants of an orthotropic magnesium alloy. On the other hand, if the SNN is built from a database containing only variants of the orthotropic magnesium alloy, its accuracy is of the same order as that obtained for the titanium alloy.

It can be concluded that combining very dissimilar materials in the same database is not recommended. Instead, a dedicated database per type of material, or per variations of the same alloys can produce a complete yield surface using very few testing points, and within a fraction of a second on a standard laptop.

CRediT authorship contribution statement

Chady Ghnatios: Conceptualization, Data curation, Formal analysis, Funding acquisition, Investigation, Methodology, Project administration, Resources, Software, Validation, Visualization, Writing – original draft, Writing – review & editing. **Oana Cazacu:** Conceptualization, Formal analysis, Funding acquisition, Investigation, Methodology, Project administration, Supervision, Validation, Writing – original draft, Writing – review & editing. **Benoit Revil-Baudard:** Conceptualization, Data curation, Formal analysis, Investigation, Software, Writing – original draft, Writing – review & editing. **Francisco Chinesta:** Conceptualization, Formal analysis, Funding acquisition, Investigation, Methodology, Project administration, Supervision, Writing – original draft, Writing – review & editing.

Declaration of competing interest

The authors declare that they have no known competing financial interests or personal relationships that could have appeared to influence the work reported in this paper.

Data availability

A data generator is described in the paper.

Appendix. CPB identified parameters

The CPB parameters used for the selected four nominal materials are given below:

- Titanium T40:

$$\mathbf{C} = \begin{bmatrix} 1 & -0.07076 & 0.014048 & 0 & 0 & 0 \\ -0.07076 & 1.192942 & 0.0623 & 0 & 0 & 0 \\ 0.014048 & 0.0623 & 1.0249 & 0 & 0 & 0 \\ 0 & 0 & 0 & 1.26677 & 0 & 0 \\ 0 & 0 & 0 & 0 & 1.26677 & 0 \\ 0 & 0 & 0 & 0 & 0 & 1.26677 \end{bmatrix}$$

$$k = -0.32544$$
$$a = 2$$

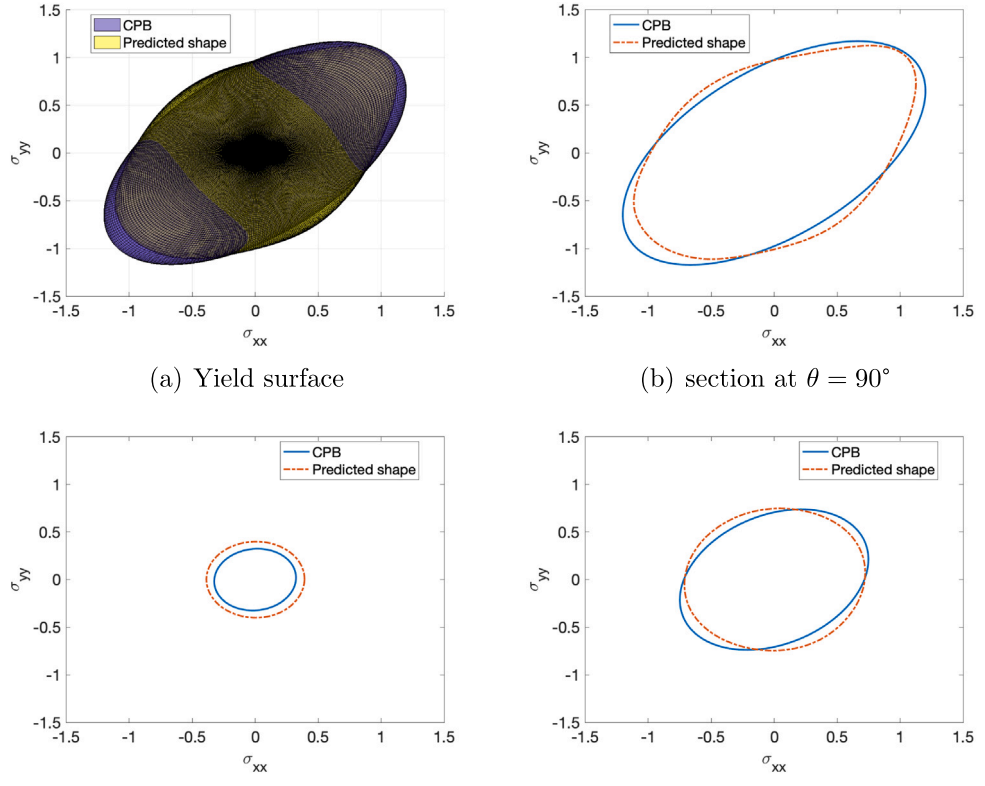

(a) Yield surface (b) section at $\theta = 90°$

(c) section at $\theta = 30°$ (d) section at $\theta = 60°$

Fig. 11. Comparison between the true (CPB) yield surface and the generated yield surface for a material selected from the testing set (variant of a von Mises material), obtained using the proposed methodology with a database containing realizations of 4 HCP materials and eight measurement points $\mathbf{X}_8$.

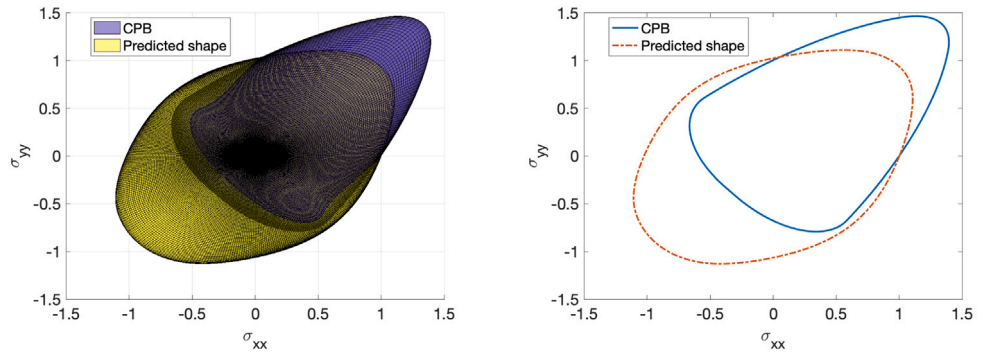

(a) Yield surface

(b) section at $\theta = 90°$

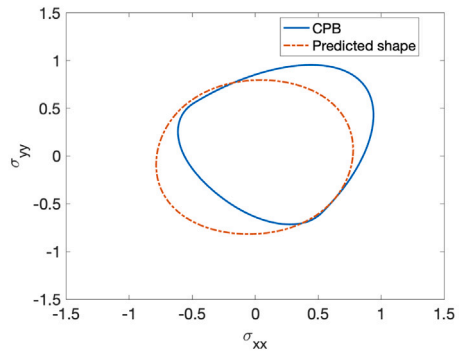

(c) section at $\theta = 30°$

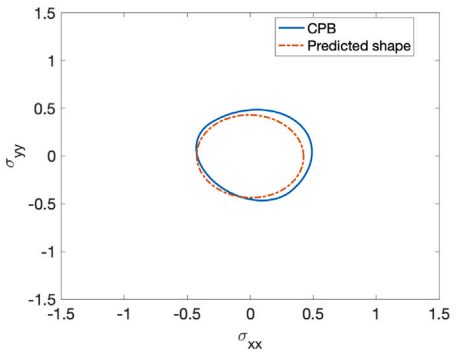

(d) section at $\theta = 60°$

Fig. 12. Comparison between the true (CPB) yield surface and the generated yield surface for a material selected from the testing set (variant of a HCP magnesium material), obtained using the proposed methodology with a database containing realizations of 4 HCP materials and five measurement points $\mathbf{X}_5$.

- von Mises :

$$\mathbf{C} = \begin{bmatrix} 1 & 0 & 0 & 0 & 0 & 0 \\ 0 & 1 & 0 & 0 & 0 & 0 \\ 0 & 0 & 1 & 0 & 0 & 0 \\ 0 & 0 & 0 & 1 & 0 & 0 \\ 0 & 0 & 0 & 0 & 1 & 0 \\ 0 & 0 & 0 & 0 & 0 & 1 \end{bmatrix}$$

$$k = 0$$
$$a = 2$$

- isotropic HCP Titanium material:

$$\mathbf{C} = \begin{bmatrix} 1 & 0 & 0 & 0 & 0 & 0 \\ 0 & 1 & 0 & 0 & 0 & 0 \\ 0 & 0 & 1 & 0 & 0 & 0 \\ 0 & 0 & 0 & 1 & 0 & 0 \\ 0 & 0 & 0 & 0 & 1 & 0 \\ 0 & 0 & 0 & 0 & 0 & 1 \end{bmatrix}$$

$$k = -0.9$$
$$a = 2$$

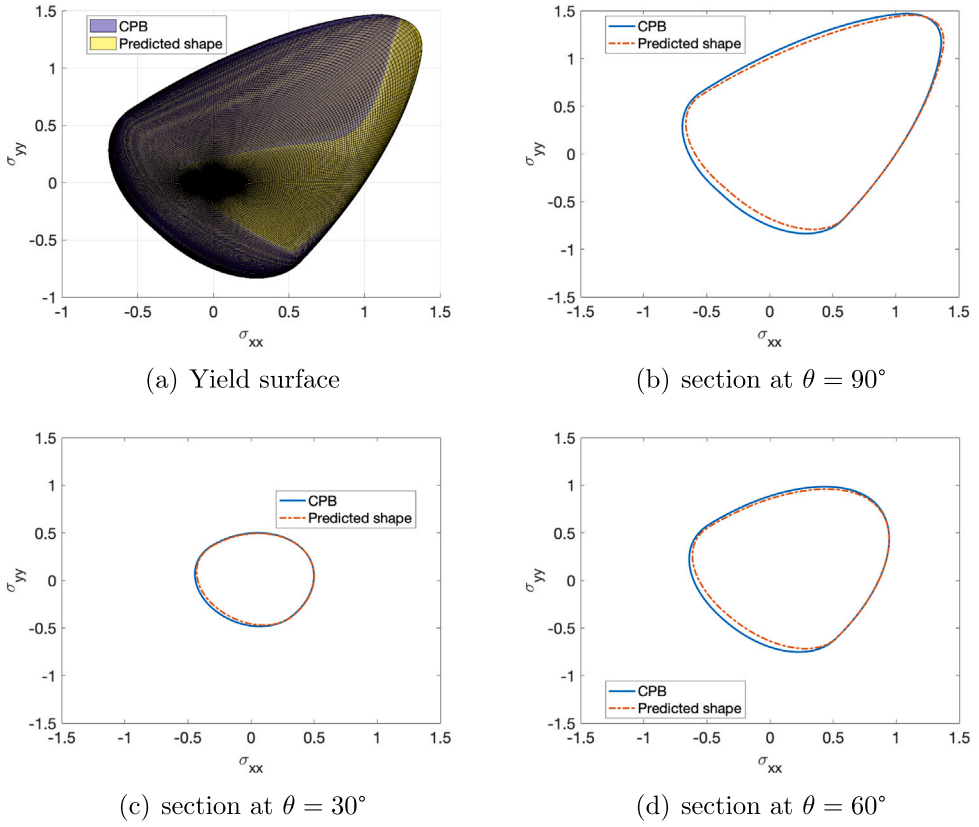

(a) Yield surface (b) section at $\theta = 90°$

(c) section at $\theta = 30°$ (d) section at $\theta = 60°$

Fig. 13. Comparison between the true (CPB) yield surface and the generated yield surface for variant of a magnesium alloy selected from the testing set, obtained using the proposed methodology with a database containing only realizations of magnesium materials and five measurement points $\mathbf{X}_5$.

- Magnesium:

$$\mathbf{C} = \begin{bmatrix} 1 & -0.168 & 0.098 & 0 & 0 & 0 \\ -0.168 & 1.09 & 0.243 & 0 & 0 & 0 \\ 0.098 & 0.243 & 3.342 & 0 & 0 & 0 \\ 0 & 0 & 0 & 0.73 & 0 & 0 \\ 0 & 0 & 0 & 0 & 7.3 & 0 \\ 0 & 0 & 0 & 0 & 0 & 7.74 \end{bmatrix}$$

$$k = -0.625$$
$$a = 2$$

References

Allen, A.E.A., Tkatchenko, A., 2022. Machine learning of material properties: Predictive and interpretable multilinear models. Sci. Adv. 8 (18), eabm7185. http://dx.doi.org/10.1126/sciadv.abm7185, URL https://www.science.org/doi/abs/10.1126/sciadv.abm7185.

Barlat, F., Aretz, H., Yoon, J., Karabin, M., Brem, J., Dick, R., 2005. Linear transfomation-based anisotropic yield functions. Int. J. Plast. 21 (5), 1009–1039. http://dx.doi.org/10.1016/j.ijplas.2004.06.004, URL https://www.sciencedirect.com/science/article/pii/S0749641904001160.

Cazacu, O., Barlat, F., 2004. A criterion for description of anisotropy and yield differential effects in pressure-insensitive metals. Int. J. Plast. 20 (11), 2027–2045. http://dx.doi.org/10.1016/j.ijplas.2003.11.021, Daniel C. Drucker Memorial Issue.

Cazacu, O., Plunkett, B., Barlat, F., 2006. Orthotropic yield criterion for hexagonal closed packed metals. Int. J. Plast. 22 (7), 1171–1194. http://dx.doi.org/10.1016/j.ijplas.2005.06.001.

Cazacu, O., Revil-Baudard, B., Chandola, N., 2019. Plasticity-Damage Couplings: From Single Crystal to Polycrystalline Materials, first ed. In: solid Mechanics and Its Applications, vol. 253, Springer.

Chinesta, F., Ladeveze, P., Cueto, E., 2011. A short review on model order reduction based on proper generalized decomposition. Arch. Comput. Methods Eng. 18 (4), 395–404. http://dx.doi.org/10.1007/s11831-011-9064-7.

Fuhg, J.N., Fau, A., Bouklas, N., Marino, M., 2022a. Elasto-Plasticity with Convex Model-Data-Driven Yield Functions. Working Paper or Preprint, URL https://hal.science/hal-03619186.

Fuhg, J.N., van Wees, L., Obstalecki, M., Shade, P., Bouklas, N., Kasemer, M., 2022b. Machine-learning convex and texture-dependent macroscopic yield from crystal plasticity simulations. Materialia 23, 101446. http://dx.doi.org/10.1016/j.mtla.2022.101446, URL https://www.sciencedirect.com/science/article/pii/S2589152922001296.

Hill, R., 1948. A theory of the yielding and plastic flow of anisotropic metals. Proc. R. Soc. Lond. Ser. A Math. Phys. Eng. Sci. 193, 281–297.
Hill, R., 1979. Theoretical plasticity of textured aggregates. Math. Proc. Camb. Phil. Soc. 85 (1), 179–191. http://dx.doi.org/10.1017/S0305004100055596.
Ibáñez, R., Abisset-Chavanne, E., González, D., Duval, J.-L., Cueto, E., Chinesta, F., 2019. Hybrid constitutive modeling: Data-driven learning of corrections to plasticity models. Int. J. Mater. Form. 12 (4), 717–725. http://dx.doi.org/10.1007/s12289-018-1448-x.
Kingma, D.P., Ba, J., 2014. Adam: A method for stochastic optimization. CoRR abs/1412.6980.
Kirchdoerfer, T., Ortiz, M., 2016. Data-driven computational mechanics. Comput. Methods Appl. Mech. Engrg. 304, 81–101.
Mises, R.V., 1928. Mechanik der plastischen Formänderung von Kristallen. ZAMM - J. Appl. Math. Mech. / Z. Angew. Math. Mech. 8 (3), 161–185. http://dx.doi.org/10.1002/zamm.19280080302, URL https://onlinelibrary.wiley.com/doi/abs/10.1002/zamm.19280080302.
Revil-Baudard, B., Cazacu, O., Massoni, E., 2021. Room-temperature plastic behavior and formability of a commercially pure titanium: Mechanical characterization, modeling, and validation. Int. J. Solids Struct. 228, 111121.